LA-UR- 03-1045

Approved for public release; distribution is unlimited.

Title: Proceedings of the NEDPC 2003

Author(s): Christopher L. Morris,* Thomas J. Asaki,* Jeffrey D. Bacon,* John A. Balog,* Stuart Baker,** Jan G. Boissevain,* Kevin L. Buescher,* Dominic J. Cagliostro,* Deborah J. Clark,* David A. Clark,* David D. Clark,* Eduardo T. Campos,* Camilo J. Espinoza,* Joshua Craft,* Norman T. Gray,* George Greene,†† Robert Gallegos,* Albert Hanson,†† Gary E. Hogan,* Brian Hollander,* John W. Hopson Jr.,* Steven A.

Submitted to: Classification Review Designator

Los Alamos
NATIONAL LABORATORY

Los Alamos National Laboratory, an affirmative action/equal opportunity employer, is operated by the University of California for the U.S. Department of Energy under contract W-7405-ENG-36. By acceptance of this article, the publisher recognizes that the U.S. Government retains a nonexclusive, royalty-free license to publish or reproduce the published form of this contribution, or to allow others to do so, for U.S. Government purposes. Los Alamos National Laboratory requests that the publisher identify this article as work performed under the auspices of the U.S. Department of Energy. Los Alamos National Laboratory strongly supports academic freedom and a researcher's right to publish; as an institution, however, the Laboratory does not endorse the viewpoint of a publication or guarantee its technical correctness.

Form 836 (8/00)

Some Results from Experiment 963 (U)

Christopher L. Morris,* Thomas J. Asaki,* Jeffrey D. Bacon,* John A. Balog,* Stuart Baker, Jan G. Boissevain,* Kevin L. Buescher,* Dominic J. Cagliostro,* Deborah J. Clark,* David A. Clark,* David D. Clark,* Eduardo T. Campos,* Camilo J. Espinoza,* Joshua Craft,* Norman T. Gray,* George Greene,†† Robert Gallegos,* Albert Hanson,†† Gary E. Hogan,* Brian Hollander,* John W. Hopson Jr.,* Steven A. Jaramillo,* John A. Josef,* Deniece Korzekwa,* Craig Kruschwitz,** Kris K Kwiatkowski,* Nicholas S. P. King,* Julian D. Lopez,* Fesseha G. Mariam,* John A. McGill,† Kevin B. Morley,* C. Thomas Mottershead,* Frank Merrill,* Matthew M. Murray,* Peter D. Pazuchanics,* John E. Pearson,* Andrea Palounek,* Andrew Sanchez,* John S. Sarracino,* Stephen M. Sterbenz,* Alexander Saunders,* Joseph Scaduto,†† Richard C. Schirato,*Terry N. Thompson,* Richard T. Thompson,** Nicholaos Tsoupas,†† Joshua Tybo,** Andrew L. Sanchez*, Philip K. Tubesing*, Pete Walstrom,* Adam Whiteson,** Mark D. Wilke,* John D. Zumbro***

*Los Alamos National Laboratory, P. O. Box 1663, Los Alamos, New Mexico, 87545;
**Bechtel Nevada, Los Alamos Operations, P.O. Box 809 Los Alamos, NM 87544;
†General Atomics, P.O. Box 85608, San Diego, CA 92186-5608; ††Brookhaven National Laboratory, P.O. Box 5000, Upton, NY 11973-5000

We present radiographic data taken with 24 GeV/c protons provided by the Alternating Gradient Synchrotron at Brookhaven National Laboratory on a set of high fidelity test objects. The test objects were designed to reproduce the time dependence of areal densities predicted by hydrodynamical calculations of a primary hydrotest. The goal of this work is to determine the quantitative limits of proton radiography. (U)

Introduction

With the cessation of underground testing, considerable effort has been expended to improve x-ray technology. The most recent manifestations of this effort are the first axis of the Dual-Axis Radiographic Hydrodynamics Test (DARHT) facility and the ARIX facility[1]. These machines are producing the largest doses and smallest spot sizes ever achieved for flash radiography. Nevertheless, better information than is obtainable with x-rays is needed to answer the questions about stockpile performance to the precision required for long term stockpile certification.

The limitations of x-ray radiography and the motivation for studying proton radiography for hydrotest experiments arise from very simple considerations. The optimum mean free path, λ, for radiographing an object of a given thickness, l, is $\lambda = \frac{l}{2}$. The maximum mean-free path for x-rays occurs at energies near 4 MeV and is about 22 gm/cm^2 or a little over a centimeter of uranium. This is far from the optimum for hydrotest experiments. An alternative to x-rays is provided by hadronic rather than electromagnetic probes. The hadronic mean free path in uranium[2] is near 200 gm/cm^2 and is much better matched to hydrotest radiography than the x-ray mean free path. Consequently, the same statistical information can be obtained with a much lower incident flux of hadrons than with high energy x-rays.[3]

It is possible to take advantage of the long hadronic mean-free path by using high-energy protons as a radiographic probe. High intensities are available in short pulses using current accelerator technology. Since protons are charged, a proton beam can be distributed across a radiographic object and focused onto downstream detectors using electromagnets.[4]

The scale of experiments which can be radiographed at a given proton energy is limited by the chromatic aberrations in the magnetic lens system. Because the beam is "matched" to the lens, aberrations are dominated by the chromatic length of the lens, $\langle x|\theta\delta\rangle$. The blur due to this term can be calculated as $\Delta x = \langle x|\theta\delta\rangle \theta_0 \delta$ where Δx is the position blur, θ_0 is the multiple scattering angle for protons transmitted through the experiment, δ is the momentum spread of transmitted protons, and $\langle x|\theta\delta\rangle$ is a coefficient which is generally on the order of the length of the lens system. For a given experiment

[1] Carl Ekdahl, "Modern Electron Accelerators for Radiography", IEEE Transactions on Plasma Science, 30 (2002) 254-261.

[2] Particle Data Group, Euro. Phys. J C3 (1998) 1.

[3] C. L. Morris, et al., "A comparison of proton and x-ray thick object radiography", Defense Research Review, in press, (2004)

[4] A. Gavron, C. L. Morris, H. J. Ziock, and J. D. Zumbro, "Proton Radiography," Los Alamos National Laboratory document LA-UR-96-420.

both θ_0 and δ scale as $1/p$ where p is the beam momentum. Therefore, the chromatic blur scales as $1/p^2$ assuming the length of the lens is constant.

In a set of experiments[5] performed using the Alternating Gradient Syncrotron (AGS) at Brookhaven National Laboratory (BNL), data have been taken on a set of test objects to validate proton radiography and to compare it to X-radiography from DARHT. Both the higher momentum and lower chromatic aberrations, 24 GeV/c at AGS *vs.* 1.4 GeV/c at LANSCE, and the higher intensity, 10^{11} *vs.* 10^9 protons, allow a much broader program of experiments in support of science based stockpile stewardship (SBSS) if such beam were available for dynamic experiments. In all cases that have been studied the qualities expected from proton radiography have been verified, and in comparisons even low intensity bunches of 10^{10} protons provide a radiographic advantage over DARHT performance of a factor of between 10 and 100 in units of dose.[3]

Test Objects

In proton radiography there are two components to the attenuation, $\frac{N}{N_0}(x_0, y_0) = t_\lambda(x_0, y_0) t_{MS}(x_0, y_0)$. In this factorization approximation, the first term is due to nuclear scattering and the second is due to Coulomb multiple scattering. Here x_0 and y_0 are the coordinates at the object plane of the lens.

The first term can be obtained by a generalization of the discussion above:

$$t_\lambda(x_0, y_0) = e^{-\Lambda(x_0, y_0)},$$

where $\Lambda(x_0,y_0)$ is the attenuation-length weighted path-length integral on the trajectory that goes through the point (x_0, y_0).

Proton radiography relies on lenses to restore position resolution lost due to the Coulomb multiple scattering. The images in a two lens proton radiography system can be used to separate the loss of flux due to Coulomb multiple scattering from the loss due to nuclear scattering and allow material identification.[6] If the multiple scattering angular distribution is given by a Gaussian, the transmission through an aperture located at the Fourier point, that transmits protons with polar angles smaller than θ_c, in the lens system is given by:

[5] K. Alrick, et al., "Some Preliminary results from experiment 933", LAUR-00-4796 (2000).

[6] C. L. Morris, "A study of the effect of angular acceptance on material identification for the AHF." LAUR004795.

$$t_{MS} = \frac{1}{2}\int_0^{\theta_0} e^{-\frac{\theta^2}{2\theta_0^2}} \theta d\theta$$

$$t_{MS} = (1 - e^{-\frac{\kappa}{X(x_0,y_0)}})$$

where:

$$\theta_0 = \frac{14.1}{p\beta}\sqrt{X(x_0,y_0)}$$

$$\kappa = \frac{\theta_c^2 p^2 \beta^2}{14.1^2}.$$

Here β is the proton velocity relative to the speed of light and $X(x_0, y_0)$ is the radiation length weighted path length integral on the trajectory that goes through the point (x_0, y_0).

Hydrodynamical calculations give the volume densities, $\rho_{V_j}(r,z)$, as a function of position for each of the materials, j, where axial symmetry has been assumed so that the volume density is written in cylindrical coordinates. For proton radiography, the illumination from a chromatically matched source leads to trajectories through the object that can be written as:

$$x(z) = x_0\left(1 + \frac{z}{L_x}\right)$$

$$y(z) = y_0\left(1 + \frac{z}{L_y}\right).$$

Here, L_x and L_y are matching distances in the x and y directions respectively. These are a result of the linear angle position correlation built into the beam to cancel the first order chromatic aberrations. This is similar to the cone beam correction for x-ray radiography except for a sign change in the second term.

The path length integrals separated for each material j, $X_j(x_0,y_0)$ and $\Lambda_j(x_0,y_0)$, are given by:

$$X_j(x_0,y_0) = \int \frac{\rho_{V_j}\left(x_0\left(1+\frac{z}{L_x}\right), y_0\left(1+\frac{z}{L_y}\right)\right)}{X_j} dz,$$

$$\Lambda_j(x_0,y_0) = \int \frac{\rho_{V_j}\left(x_0\left(1+\frac{z}{L_x}\right), y_0\left(1+\frac{z}{L_y}\right)\right)}{\lambda_j} dz.$$

where $X(x_0,y_0) = \sum_j X_j(x_0,y_0)$, and $\Lambda(x_0,y_0) = \sum_j \Lambda_j(x_0,y_0)$.

Although the volume densities encountered in a hydro test are too large to be reproduced with static materials, one can reproduce the path-length integrals by using objects

that are extended in the beam direction.[7] An ideal test object could be constructed of at least two materials and would match both of these integrals. The angular acceptance for designs for the AHF is large enough so that t_{MS} can be near unity.[6] Since the goal of this experiment was to reconstruct the densities of the heavy metal we took advantage of the simplifications that could be obtained by using a single material test object that faithfully reproduces $\Lambda(x_0, y_0)$.

It is advantageous to use a high density material for the test object in order to keep the length as short as possible in order to minimize uncertainties due to blur and alignment associated with the extended length of the object. Previous experiments have suffered from difficulties due to the non uniformity of machinable tungsten alloys. The best high density choices are the base metals, gold and platinum. We choose to use gold for these tests, which has a density of ρ_{Au} = 19.3 gm/cm^3, has purity exceeding 99.9% in standard form, is easily cast and machined. The test objects were constructed by interpolating the surface:

$$z(x_0\left(1+\frac{z}{L_x}\right), y_0\left(1+\frac{z}{L_y}\right)) = \frac{\Lambda(x_0, y_0)\lambda_{Au}}{\rho_{Au}}$$

onto a rectilinear grid. This surface was used to produce a slightly oversized graphite mold. This rough form was cast and machined to its final shape using a computer-controlled three-axis milling machine. The machining was performed by profiling the outer surface with a set of ball endmills with decreasing diameters as the machining approached the final surface. The maximum reach of a given diameter end mill defined the fidelity to which the object could be machined. The outer profile of the objects was machined with a 6.35 mm diameter endmill, while the inner details were machined with a 3.175 mm diameter endmill. Because there are expected to be some significant effects from the machining process near edges[8] full metrology of the final object is planed though not yet completed.

Experiment

Protons were provided by the AGS at BNL in single bunches, on demand, of up to 2_10^{11} protons per bunch. The beam momentum chosen for the work reported here was 24 GeV/c. The magnetic optics for this experiment consisted of the beam transport line (line U), a diffuser which was fixed at 6 mm thick of tantalum, a matching section consisting of and an identity lens.[9] I schematic of this system is shown in Figure 1). Beam

---

[7] Douglas Venable, "The Feasibility of Studying Imploding Weapons Using Flash Radiography," Los Alamos Report: GMX-7-502 (1952).

[8] Tom Asaki and Kevin Vixie, contribution to this conference.

[9] C. Thomas Mottershead and John D. Zumbro, "Magnetic Optics for Proton Radiography", Proceedings of the 1997 Accelerator Conference, (1998) 1397-1399

positions were measured at two locations upstream of the diffuser and two locations downstream of the diffuser with a set of CCD camera-imaged phosphors, and by two hydrogen ion chambers.[10] Integrated beam fluxes were measured using a set of integrating current transformers, two upstream of the target and one in the image location.

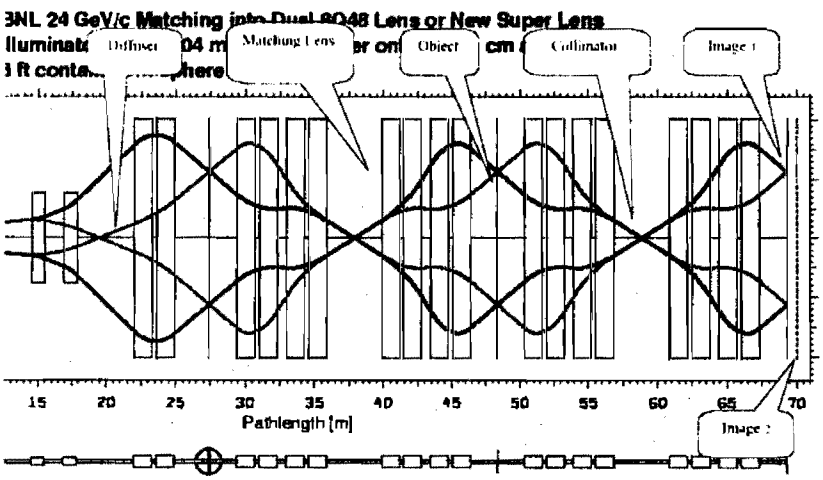

n	name	Env[cm]	a[cm]	Length[m]	G[T/m]	Bpole[kG]	Path[m]
1	difax	1.52	3.81	14.5766			14.577
2	ZQ1 3Q36	1.79	3.81	0.9474	19.7336	7.518	15.524
3	zap	2.46	3.81	1.3810			16.905
4	ZQ2 3Q36	3.21	3.81	0.9474	19.7336	7.518	17.8525

Figure 1) schematic layout of the matching section and lens.

The redundant beam monitoring proved to be important in the data analysis. The cameras that imaged the phosphors, the most precise beam position measurement, failed to function properly for about half of the test object data. Beam position corrections for this fraction of the data were made using the hydrogen ion chamber information.

A remotely-controlled translation stage (background stage) was mounted 1 meter upstream of the object location which allowed a 15-cm block of tungsten, a 1cm diameter 15-cm long rod of tungsten, a 15-cm thick tungsten block with a 1-cm diameter hole, and a open position to be scanned horizontally across the object location. These were used to measure the scatter (the sum of light and proton) backgrounds in the images.

A remotely-controlled stage that allowed two rotations and translation in both directions in the plane normal to the beam was placed at the object location. This stage allowed each of the test objects needed for the experiment to be placed in the beam and aligned without making an entry into the beam line. This was crucial for obtaining the amount of data needed to characterize systematic uncertainties and to perform all of the calibrations needed for this experiment in the allocated time.

---

[10] Larry Schultz, K. K. Kwiatkowski, C. L. Morris, A. Saunders, G. E. Hogan, F. E. Merrill, and K. B. Morley, "A narrow gap ion chamber for beam motion correction in proton radiography experiements", Nuclear Instruments and Methods in Physics Research A, **508** (2003) 220-226.

There was a remotely-controlled rotational stage at the Fourier (collimator) point in the lens system that allowed a phosphor screen or one of a set of four collimators to be placed in the beam. The data presented in this work were all obtained with one collimator with a nominal angular acceptance of 6.68 mrad.

We used two detectors in the image plane. One was located at the nominal image location. The other could be moved from 1 cm to 30 cm downstream of the fixed detector to image at a different energy/ position in the object plane. The second camera increased the dynamic range of the system and demonstrates how lower energy machines may be used for hydrotest radiography than were proposed in the AHF project. Each of the detectors imaged a 3_3 array of 40_40_~1 mm thick lutetium oxyorthosilicate (LSO) radiation to light converters that imaged the beam transmitted through the object and the lenses.

Data processing

A number of corrections were made to the raw images. Amplifier baseline and dark current were subtracted. The "stars" resulting from direct proton interactions (which affects > 1% of the pixels) were replaced with an average value from surrounding pixels. The image of each tile was corrected for a fraction of the light which carries no spatial information, but rather glows with intensity proportional to the total flux incident on the tile, a 2% correction.[11] Light scatter, beam halo, and off momentum scattered protons and other charged particles can all cause diffuse background in the image plane. The data were corrected for this "scatter" background using a previously described method for long range blur corrections.[12] The parameters of this correction were obtained by radiographing different thicknesses of the gold step wedge through the different beam conditioners on the background stage, and adjusting the length and fraction of the long range blur to give the best results. We found that a long range blur of 2 cm range with a fraction of 4% reproduced both the step wedge and thick object data remarkably well. These are the parameters that were used throughout the analysis.

Data were taken with the step wedge moved though the object plane using the object stage. This procedure gave a range of gold thicknesses at different positions across the image plan. Data were also taken as a function of lens setting. No significant dependence to transmission was observed as a function of position or momentum across the dynamic range of the test objects. These results show that transmission through the full dynamic range of the test object can be adequately described using only three parameters, the beam emittance, an effective X_0, and the effective λ for gold. The beam emittance parameter accounts for the angular spread in the beam due to its intrinsic emittance and to material in the beam (windows, air, etc.).

---

[11] Chris Morris, et. al., "Tile Glow Correction," LANL, LLNL, and Bechtel Nevada, private communication (2002) https://prad.lanl.gov/Notes/Restricted/NoLA-UR/TileGlow.pdf.

[12] N. S. P. King, K. B. Morley, C. L. Morris, and P. Pazuchanics, "Long Range Blur Correction to Proton Radiography Data", LA-UR-01-0127 (2001).

Through the course of the experiment about 200 beam exposures were taken. These were each analyzed as described above and fitted with a two dimensional Gaussian. The average of the residual of all of these fits was used as a fixed pattern noise correction of each of the data runs. The upstream beam monitor data was used to estimate the width and position for each beam pulse. The intensity of each beam pulse was measured using the upstream transformers. Each radiograph was divided by a two dimensional Gaussian, whose parameters were obtained from this data, giving absolutely normalized transmission data. The beam pulses analyzed in the same fashion were used to estimate the uncertainty associated with this procedure. The uncertainty in the normalization was about 1.5%, and systematic uncertainties across the image plane (flatness) were less than 1% in general.

Areal densities were calculated from the test object data by first dividing by a simulated radiograph of the overburden (high explosives etc), then inverting the equation that was used to fit the stepwedge data pixel by pixel. This resulted in areal densities that were zero outside of the field of view, and allowed the volume densities to be calculated using a conditioned Abel inversion technique. These steps are illustrated in Figure 2.

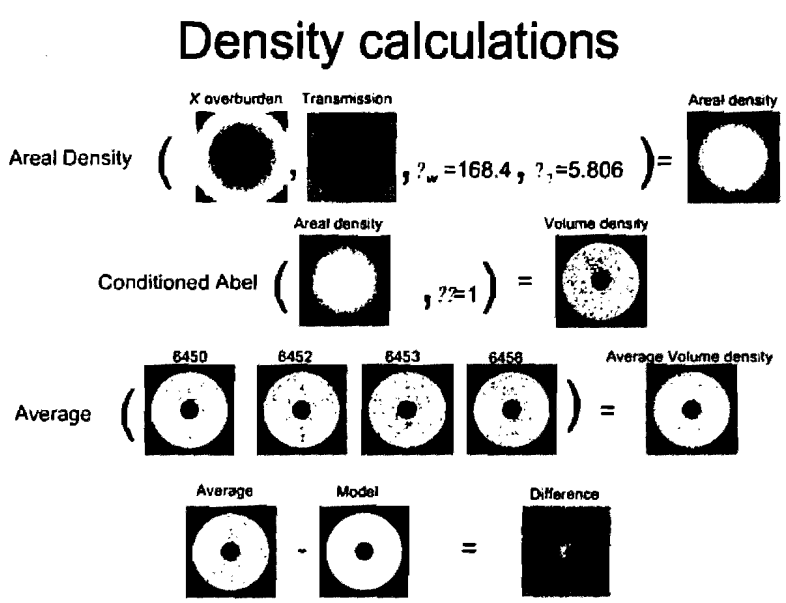

Figure 2) Analysis of data taken on the FTO illustrating the density analysis and error estimate.

Several radiographs were made of each of the test objects. Both the root mean square (rms) difference across the data set for each object and the fraction difference between the average measurement and the model are similar to previous results obtained with the French Test Object (FTO) shown in Figure 2. The plot shows a histogram of densities in the 100 micron squared pixels across the field of view measured in four different runs, and a histogram obtained by averaging all four runs. Numerical values for the average and standard deviation of densities in the tungsten density are shown below the plot. The

actual density was 19.3 gm/cm^3. Finally, the integrated mass of the tungsten is compared for the individual runs and the actual value in the table at the right of the figure.

FTO analysis reproducibility

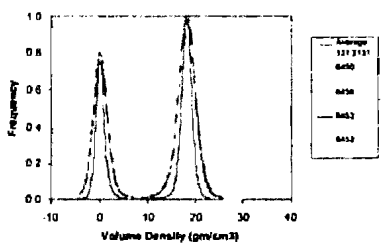

run	?	?
	gm/cm^3	gm/cm^3
6450	18.1604	2.1443
6452	18.1056	2.1053
6453	18.1259	2.0790
6456	18.2224	2.1968
Average	18.1443	1.4133
Stdev	0.051	

Run	Mass
	gm
6450	6978.5
6452	6960.5
6453	6976.5
6455	7004.5
Actual	6903
Average	6979.5
Average/actual	1.011
Stdev/Average	0.0026

Density measurements
- Reproducibility <1%
- Precision ~1%

Figure 3 Quantitative FTO results from experiment 955. These are illustrative of the results from experiment 963.

Given the caveat that the metrology on the objects is not yet completed, we can say that the agreement across the flat regions in density and averaged across the dynamic range present by the objects is well better than 1%. Near the boundaries and in the outer parts of the object the agreement is worse. Some of this discrepancy may be due to the machining process, which leaves extra material in regions with structure and near edges, and some may be due to radiographic blur. The resolution of this issue waits completing the metrology.

Conclusions

In conclusion, we have described a new technique for construction high fidelity test objects. We have used this technique to produce a set of test objects that reproduce the densities predicted by a hydrocode calculation for a specific hydrotest at three different times. Using a set of beam diagnostics, test objects, and various calibration techniques we taken a set of calibration data and developed procedures that result in sub-one percent density reconstructions in the flat high density regions of these objects. Discrepancies near boundaries and in lower density regions are being investigated. We have not ad-

dressed the influence of multiple materials on this inference. Although this is expected to be a small effect on the analysis, we intend to further study this problem using Monte Carlo transport models.

Acknowledgements

This work has been supported by the NNSA at the DOE. We would like to express or appreciation for the management and operations staff of the AGS at Brookhaven National laboratory, whose dedicated work made this experiment possible, and to LANL management, who encouraged and funded this work.